



Stabilization of pentazolate anions in high-pressure compounds Na_2N_5 , NaN_5 and in sodium pentazolate framework $\text{NaN}_5\cdot\text{N}_2$

Journal:	<i>Dalton Transactions</i>
Manuscript ID	DT-ART-03-2021-000722.R1
Article Type:	Paper
Date Submitted by the Author:	06-Apr-2021
Complete List of Authors:	Bykov, Maxim; Earth and Planets Laboratory Carnegie Institution for Science Bykova, Elena EB; Earth and Planets Laboratory Carnegie Institution for Science Chariton, Stella SC; Center for Advanced Radiation Sources University of Chicago Prakapenka, Vitali; Center for Advanced Radiation Sources University of Chicago Batyrev, I.; US Army Research Laboratory RDRL-WML-B Mahmood, Mohammad F. MFM; Howard University Goncharov, Alexander F. AFG; Earth and Planets Laboratory Carnegie Institution for Science

ARTICLE

Stabilization of pentazolate anions in high-pressure compounds Na_2N_5 , NaN_5 and in sodium pentazolate framework $\text{NaN}_5\cdot\text{N}_2$

Received 00th January 20xx,
Accepted 00th January 20xx

DOI: 10.1039/x0xx00000x

Maxim Bykov,^{a,b,*} Elena Bykova,^b Stella Chariton,^c Vitali B. Prakapenka,^c Iskander G. Batyrev,^d Mohammad F. Mahmood,^a Alexander F. Goncharov^b

Synthesis and characterization of nitrogen-rich materials is important for the design of novel high energy density materials due to extremely energetic low-order nitrogen-nitrogen bonds. The balance between energy output and stability may be achieved if polynitrogen units are stabilized by resonance as in *cyclo-N₅⁻* pentazolate salts. Here we demonstrate the synthesis of three oxygen-free pentazolate salts Na_2N_5 , NaN_5 and $\text{NaN}_5\cdot\text{N}_2$ from sodium azide NaN_3 and molecular nitrogen N_2 at ~ 50 GPa. $\text{NaN}_5\cdot\text{N}_2$ is a metal-pentazolate framework (MPF) obtained via a self-templated synthesis with nitrogen molecules being incorporated into the nanochannels of the MPF. Such self-assembled MPFs may be common for a variety of ionic pentazolate compounds. The formation of Na_2N_5 demonstrates that *cyclo-N₅⁻* group can accommodate more than one electron and indicates the great accessible compositional diversity of pentazolate salts.

Introduction

Pentazolate anion *cyclo-N₅⁻*, the recently discovered all-nitrogen structural unit has attracted much attention due to potential application of nitrogen-rich compounds as high-energy density materials^{1–4}. Although this five-membered ring is formed by the high-energy nitrogen-nitrogen bonds, the aromaticity provides good thermal stabilities of pentazolate salts. In 2017 the pentazolate anion was generated by direct cleavage of the C–N bond in a multisubstituted arylpentazole using *m*-chloroperbenzoic acid and ferrous bisglycinate and stabilized in a compound $(\text{N}_5)_6(\text{H}_3\text{O})_3(\text{NH}_4)_4\text{Cl}^3$. Consequently, a series of metal pentazolate hydrates including $[\text{Na}(\text{H}_2\text{O})(\text{N}_5)_2]\cdot 2\text{H}_2\text{O}$, $[\text{M}(\text{H}_2\text{O})_4(\text{N}_5)_2]\cdot 4\text{H}_2\text{O}$ (M=Mn, Fe and Co), and $[\text{Mg}(\text{H}_2\text{O})_6(\text{N}_5)_2]\cdot 4\text{H}_2\text{O}$ were synthesized^{1,2}. In all these salts containing the isolated *cyclo-N₅⁻*, large amounts of coordinated water molecules were contained in the crystal structure, which played an irreplaceable role in stabilizing the *cyclo-N₅⁻* anion through extensive hydrogen bond interactions. A series of pentazolate frameworks like AgN_5 , or $\text{Cu}(\text{N}_3)(\text{N}_5)$ and

$\text{Na}_{46}\text{N}_{240}\text{O}_{15}$ were obtained in ion exchange reactions with $[\text{Na}(\text{H}_2\text{O})(\text{N}_5)]\cdot 2\text{H}_2\text{O}^{5–7}$. In these water-free salts, the stabilization of *cyclo-N₅⁻* is achieved by its coordination to metals and π - π stacking interactions⁸. The $\text{Na}_{46}\text{N}_{240}\text{O}_{15}$ compound has an unprecedented zeolitic architecture with $\text{Na}_{20}\text{N}_{60}$ and $\text{Na}_{24}\text{N}_{60}$ nanocages indicating a great potential for the synthesis of other metal-pentazolate frameworks⁷.

At the same time, the synthetic route to pentazolate anion was approached from a completely different perspective. Due to the great stability of *cyclo-N₅⁻*, this structural unit emerges in ionic high-pressure polynitrides. Steele *et al.* synthesized cesium pentazolate CsN_5 in a one-step reaction between CsN_3 and N_2 in a diamond anvil cell at ~ 60 GPa⁹. Similarly, LiN_5 was synthesized from elements at 45 GPa and appeared to be metastable at ambient conditions¹⁰. Various metal pentazolates (of Na, K, Rb, Be, Mg, Ba, Al, Ga, Sc, Y, Zn) were recently predicted using modern structure search algorithms, but not yet discovered experimentally^{11–18}. Here we studied the reactions between NaN_3 and nitrogen in laser-heated diamond anvil cells attempting to extend the series of water and oxygen-free alkali-metal pentazolates. Surprisingly, in addition to expected simple sodium pentazolate salt NaN_5 , we have also synthesized never predicted previously, complex pentazolate framework structure with incorporated dinitrogen molecules $\text{NaN}_5\cdot\text{N}_2$ as well as sodium-rich pentazolate Na_2N_5 . Synthesis of complex $\text{NaN}_5\cdot\text{N}_2$ demonstrates high-pressure self-templated approach to polynitrides.

Results and discussion

^a Department of Mathematics, Howard University, Washington, DC 20059, USA

^b The Earth and Planets Laboratory, Carnegie Institution for Science, Washington, DC 20015, USA

^c Center for Advanced Radiation Sources, University of Chicago, Lemont, IL 60437, USA

^d U.S. Army Research Laboratory, RDRL-WML-B, Aberdeen Proving Ground, Maryland 21005, United States

† Electronic Supplementary Information (ESI) available: CSD numbers: NaN_5 , 2051780; NaN_7 , 2051781; 2075304 Na_2N_5 . Crystallographic Tables, Experiment Summary, Calculated and experimental Raman spectra for Na_2N_5 and NaN_5 , details of single-crystal multigrain data analysis, calculated phonon dispersion curves of NaN_5 . See DOI: 10.1039/x0xx00000x

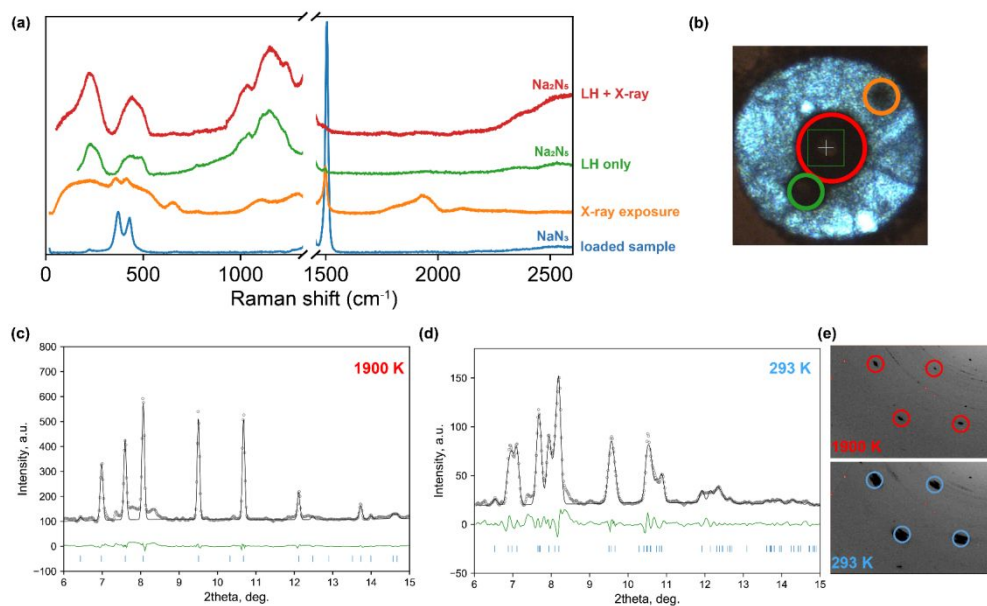


Figure 1. (a) Raman spectra collected at different positions of the NaN_3 sample (sample #1) compressed up to ~ 50 GPa. Colour codes correspond to Fig. 1b. (b) Microscopic image of the sample chamber at ~ 50 GPa. Red circle shows an area, where the sample was laser-heated, and X-ray exposed before the collection of the Raman spectrum. Green area – was laser-heated only, orange area was subject to X-ray exposure during 20 min at 37 keV. (c) Le-Bail fit of the diffraction pattern collected during laser-heating of NaN_3 at 1800 K ($P6/m$, $a = 4.8457(6)$, $c = 2.6289(8)$ Å). (d) Le-Bail fit of the diffraction pattern collected after laser-heating of NaN_3 (Pm , $a = 4.781(10)$ Å, $b = 2.5873(7)$ Å, $c = 4.934(12)$ Å, $\beta = 119.6(3)^\circ$) (e) Comparison of the diffraction patterns of hot and temperature-quenched samples.

Synthesis of Na_2N_5 by high-pressure high-temperature decomposition of NaN_3

First, we discuss the high-pressure behavior of pure NaN_3 in the experiment where no molecular nitrogen was added to the sample chamber (sample #1). Non-heated NaN_3 at ~ 50 GPa produces a very weak diffraction pattern with a few broad peaks, which makes its unambiguous indexing impossible as has already been reported before¹⁹. Although some high-pressure polymorphs of NaN_3 were predicted to be thermodynamically stable at these conditions, their formation can be prohibited by the large kinetic barriers²⁰. It should be noted that NaN_3 is sensitive to the hard X-ray radiation, which is evidenced by the darkening of the sample and appearance of new broad Raman bands (Fig. 1). X-ray exposure does not induce crystallization of the new product, which is apparently amorphous in nature (Fig. S1) and may contain new types of N-N bonds formed because of the interactions between azide ions. The Raman spectrum of the X-ray induced product agrees with the Raman spectrum of NaN_3 reported by Eremets *et al.*²¹, who compressed NaN_3 without exposing it to hard X-rays. This suggests that X-ray and laser-induced photochemical processes are similar.

To overcome the kinetic barriers and to crystallize new compounds, the sample was laser-heated at ~ 50 GPa. At high temperature of ~ 1800 K the strongest peaks on the diffraction pattern can be very well indexed with the hexagonal unit cell $a = 4.8380(6)$, $c = 2.6009(8)$ Å (Fig. 1c). On cooling the sharp peaks

split indicating the symmetry lowering (Fig. 1e). Structure refinement against single-crystal X-ray diffraction dataset of the temperature-quenched sample revealed the composition of the new phase as Na_2N_5 . It crystallizes in the monoclinic space group Pm (No. 6) with $a = 4.781(10)$ Å, $b = 2.5873(7)$ Å, $c = 4.934(12)$ Å, $\beta = 119.6(3)^\circ$ at ~ 50 GPa. Nitrogen atoms are forming *cyclo*- N_5 rings stacked along the b -axis as shown in the Fig. 2b. Sodium atoms form a hexagonal sublattice and define pseudo-hexagonal symmetry of Na_2N_5 . Due to the presence of only one N_5 ring in the unit cell, the sixfold rotation axis is a forbidden symmetry operation in Na_2N_5 at ambient temperature. Nevertheless, the lattice parameters show no monoclinic distortion at high temperature suggesting that hexagonal symmetry is fully restored, probably, due to the orientational disorder of N_5 groups.

Interestingly, the formal charge on the N_5 anion is -2, which means that the Hückel $4n+2$ rule is not fulfilled. Therefore, it can be expected that an extra electron partially filling the antibonding orbitals of *cyclo*- N_5 will lead to metallic properties of Na_2N_5 . The calculated phonon dispersion curves for Na_2N_5 exhibit no imaginary frequencies demonstrating the dynamic stability of this compound (Fig. S2).

The Raman spectrum of Na_2N_5 is shown on the Fig. 1a. It is characterized by the disappearance of strong peak around 1500 cm^{-1} that corresponds to stretching vibrations of azide ion and the emergence of broad bands centered around 230 , 440 and 1160 cm^{-1} at ~ 50 GPa.

This product is not sensitive to the X-ray radiation like the starting material as the Raman spectra of X-ray exposed and not exposed samples match very well (Fig. 1a).

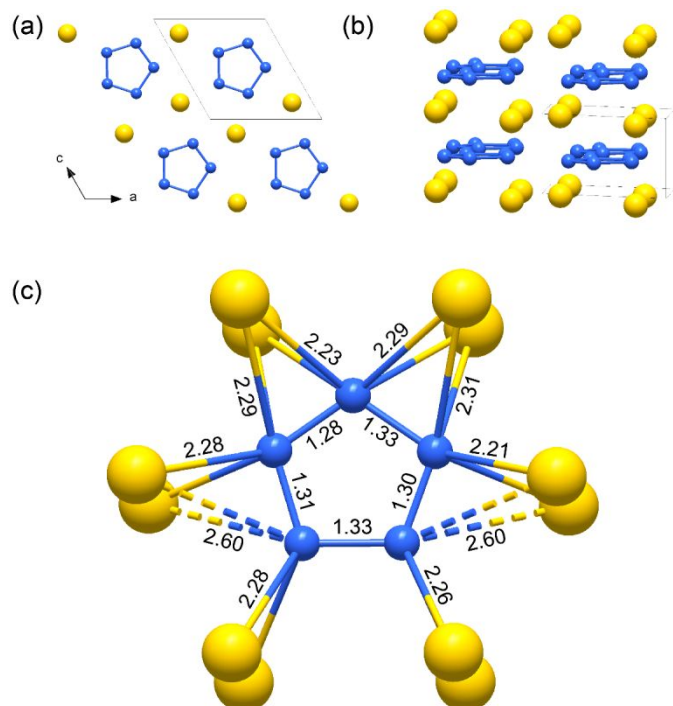


Figure 2. (a), (b) The crystal structure of $Pm\ Na_2N_5$ at 50 GPa in different projections. Na and N atoms are shown in yellow and blue respectively. (c) Coordination of *cyclo*- N_5 ring by Na atoms. Distances are given in Å. E.s.d. values of bond distances can be found in supplementary *cif* files.

Synthesis of sodium pentazolate NaN_5 and sodium pentazolate framework $NaN_5 \cdot N_2$

Laser-heating of $NaN_3 + N_2$ sample (sample #2) at ~ 52 GPa and 2200(200) K results in the formation of a series of novel Na-N compounds. Due to the intrinsic inhomogeneity of the sample, the Na:N ratio varies across the sample chamber. In the bulk of the NaN_3 piece, the Na:N ratio is close to 1:3, while on the border between NaN_3 and N_2 one can expect the formation of phases with $N:Na > 3$. This inhomogeneity, typical for high-pressure DAC experiments, makes the synthesis of phase-pure samples challenging, but at the same time allows to probe wide compositional interval in one experiment^{22–26}. In this study we combined high-resolution Raman mapping with X-ray diffraction analysis to spatially resolve various phases of the laser-heated sample. Fig. 3a, b shows the laser-heated sample #2. Already from the microscopic image one can recognize several visually distinct areas: semi-transparent area close to the gasket (non-heated and non-x-ray exposed NaN_3), dark material (heated and X-ray exposed area), several transparent spots in the heated area looking like “holes” in the sample and the fully transparent area filled with nitrogen. The Raman spectra collected in these areas have significantly different features. The Raman spectrum collected in the bulk of the sample is similar to that of Na_2N_5 , while the Raman spectra

collected at the positions of transparent spots (Fig. 3g) contain numerous sharp Raman peaks which indicate the formation of well-crystallized compounds. Each region of the sample was probed by synchrotron X-ray diffraction, which allowed a detailed structural analysis of all novel phases.

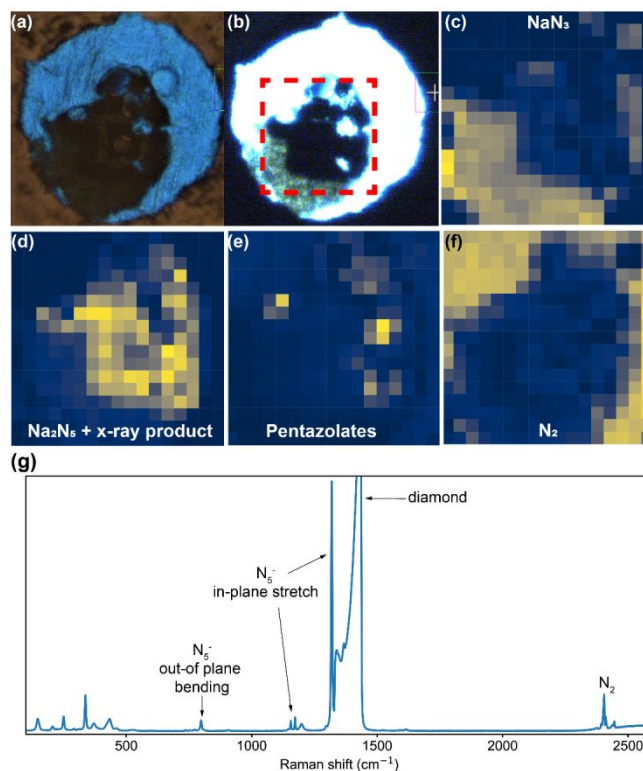


Figure 3. (a–b) The microscope photo of the Sample #2 at ~ 50 GPa after laser-heating and X-ray exposure. Red dashed square on the (b) shows the dimensions of the Raman map. (c–f) Raman maps of the reaction products. Step size for mapping is 4 μm . The brighter are the areas on the maps the stronger are the peaks in the selected regions of interest corresponding to different phases (2400 cm^{-1} for N_2 , 1500 cm^{-1} for NaN_3 , 1320 cm^{-1} for pentazolates, 1800 cm^{-1} for the X-ray product). (g) Raman spectrum of sodium pentazolate NaN_5 .

Sodium pentazolate NaN_5

X-ray diffraction analysis at the positions of the transparent heated spots of the sample#2 featuring sharp Raman peaks (Fig. 3b,e,g) revealed the formation of multiple well-crystallized single-crystal grains of new phases and it was possible to apply methods of single-crystal X-ray diffraction to solve and refine the crystal structures of the new compounds (Figs. S3,S4). The first compound with a composition NaN_5 crystallizes in an orthorhombic space group $Pmn2_1$ (No. 31) with $a = 5.455(6)$, $b = 2.836(12)$, $c = 5.662(8)$ Å, $V = 87.6(4)$ Å³ at 52.9 GPa. Full crystallographic information is provided in the supporting *cif* files and in the Table S2. Nitrogen atoms form five-membered planar rings with almost equal N-N distances ($2 \times 1.301(7)$ Å, 1.286(8) and 1.290(7) Å). No restrictions on the shape or interatomic distances were applied during the structure refinement procedure. Slight differences between N-N distances in aromatic *cyclo*- N_5^- rings are common in asymmetric or complex crystal environments^{5,27}. The refined distances are

only slightly shorter than the average N-N bond distances of the all reported *cyclo*-N₅ based salts (e.g. [Na(H₂O)(N₅)]·2H₂O: 1.316 Å; [Mg(H₂O)₆(N₅)₂]·4H₂O: 1.316 Å; [Mn(H₂O)₄(N₅)₂]·4H₂O: 1.320 Å; [Fe(H₂O)₄(N₅)₂]·4H₂O: 1.329 Å; [Co(H₂O)₄(N₅)₂]·4H₂O: 1.314 Å; [Zn(H₂O)₄(N₅)₂]·4H₂O: 1.328 Å; and (N₅)₆(H₃O)₃(NH₄)₄Cl: 1.315 Å)^{1–3,27,28}. This demonstrates that the compression mechanism of pentazolate salts primarily affects intermolecular distances leaving the N₅ units almost undistorted. Symmetric shape of *cyclo*-N₅[−] pentazolate anion agrees with its aromatic character: with 6 electrons in the delocalized π-system the Hückel rule is fulfilled. Each sodium atom is coordinated by seven pentazolate rings and each ring is coordinated with seven sodium atoms with Na-N distances varying between 2.183(8) – 2.380(11) Å as shown in the Fig. 4. Pentazolate rings stack along the *b*-axis with an offset and with the distance between ring planes of ~2.42(1) Å and 2.836(12) Å between N₅ centroids. These distances are expectedly significantly shorter than the typical π-π stacking distances at ambient conditions (e.g. ~3.47 Å in AgN₅^{5,6}), but they may play a decisive role in the stabilization of this compound²⁹.

Hitherto, high-pressure alkali metal pentazolates were synthesized in Cs-N and Li-N systems^{9,10}. CsN₅ and LiN₅ phases lack a detailed structural analysis, but both clearly have structures different from NaN₅. LiN₅ crystallizes in the monoclinic *P2* symmetry with *a* = 3.808(1) Å, *b* = 3.838(1) Å, *c* = 2.410(1) Å, and β = 99.84(1)°, yielding a volume of *V* = 34.70(4) Å³ at 73.6 GPa. CsN₅ at 60 GPa is triclinic with *V* = 349.75 Å³. Apparently quite different atomic radii of alkali metals Li, Na and Cs lead to the stabilization of different structural types.

Steele *et al.* predicted that NaN₅ with symmetry *Cm* would be thermodynamically stable at 50 GPa. This does not agree with our result, but we should note that the predicted *Cm* structure has remarkably similar structural motifs with the experimental *Pmn2*₁ structure (Fig. S5). Therefore, it is possible that these two structures can be energetically close to each other. In order to investigate this further, we have performed theoretical calculations within the framework of density functional theory, where the relative enthalpies of experimental *Pmn2*₁ and predicted *Cm* NaN₅ were considered. The *Pmn2*₁-type structure appeared to be more stable than *Cm*-NaN₅ by ~0.15 eV/atom at 50 GPa. Recently Zhou *et al.* reported the formation of *Cm*-NaN₅ by room-temperature compression of NaN₃³⁰. The compound was identified in a three-phase mixture by comparison of the theoretically predicted lattice and the experimental powder pattern, but the structure refinement was not performed. We cannot exclude the formation of metastable *Cm*-NaN₅ in the experiments of Zhou *et al.*: compression of crystalline phases at low temperatures beyond their stability range often results in formation of metastable materials³¹.

Raman spectrum collected in a sample area shown in the Fig. 3g agrees with expected modes of the pentazolate group. The strongest peak corresponding to the N₅ breathing mode is observed at 1319 cm^{−1} at 48 GPa. This is in a very good agreement with the studies of LiN₅ (~1310 at 42 GPa¹⁰) and CsN₅ (1320 cm^{−1} at 55 GPa⁹). Strong Raman peaks observed at ~800 cm^{−1} corresponds to the out-of plane vibrations of nitrogen

atoms. Theoretically calculated Raman spectrum of NaN₅ is shown on the Fig. S6. There is a fair agreement between observed and calculated modes of pentazolate groups, however an apparent complexity of the experimental Raman spectra compared to calculated as well as to LiN₅ and CsN₅ suggests that additional phases might be present in the same sample area as also confirmed by the XRD analysis (see below). It is worth noting that the Raman modes of N₅ rings in NaN₅ and Na₂N₅ differ substantially in the position and linewidth of the peaks (Fig. 1(a), Fig. 3(g)). This is because of the difference in the charge on the *cyclo*-N₅ groups, which results in dramatic dissimilarity in the electronic structure and chemical bonding.

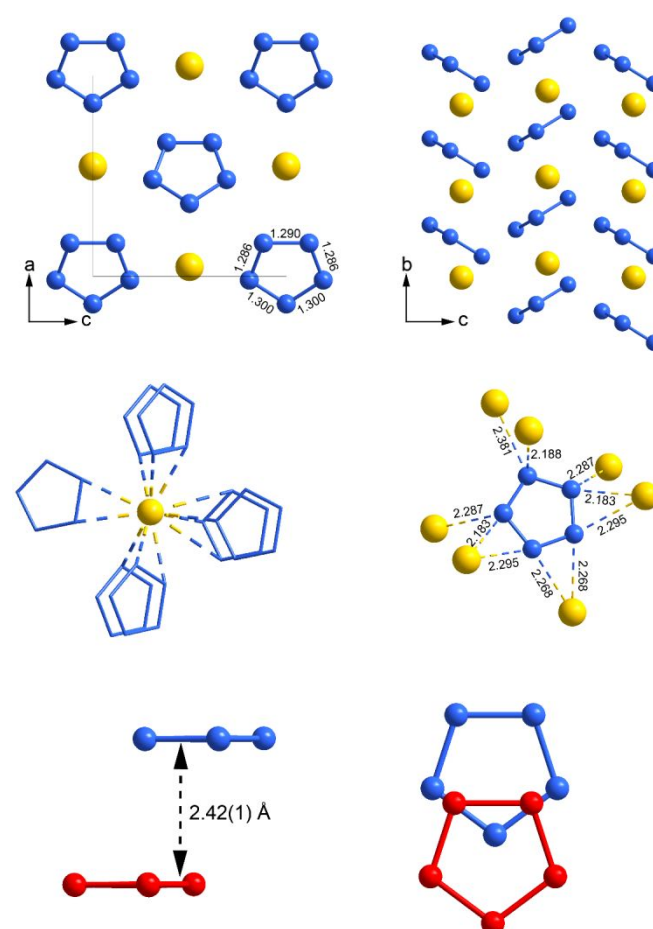


Figure 4. Crystal structure of NaN₅ at ~47 GPa shown in different projections. Yellow and blue spheres show the positions of sodium and nitrogen atoms, respectively. The lower portion of the figure shows the stacking geometry of the pentazolate rings, where stacked rings are color-coded for clarity. Distances are given in Å. E.s.d. values of bond distances can be found in supplementary cif files. Distances between N₅ ring planes are calculated using Diamond 4.6.4 software³².

Sodium pentazolate framework NaN₅·N₂ compound

Another single-crystalline phase was found together with NaN₅ at 47 GPa. It crystallizes in a monoclinic space group *P2*₁/*n* with *a* = 10.321(3), *b* = 8.672(3), *c* = 11.0409(17) Å, β = 91.70(2)°, *V* = 987.8(5) Å³. The structure contains two types of nitrogen

species: pentazolate rings cyclo-N_5^- and dinitrogen units N_2 . The unconstrained refinement of the crystal structure suggests planar shape of the N_5 units, which was constrained to planar during the final refinement for the improvement of the data/parameter ratio. The N-N distances in pentazolate vary in a range 1.26–1.32 Å and Na- N_5 distances 2.1–2.4 Å in agreement with NaN_5 . Structure solution revealed the composition of this compound as NaN_7 .

The structure of $\text{NaN}_5\cdot\text{N}_2$ is shown on the Fig. 5. Na^+ and N_5^- ions form a framework with wave-like channels running along the b -axis. Dinitrogen molecules fill these channels and possess several types of environments (Fig. 5d). Some molecules are embedded between pentazolate rings and are aligned either almost parallel or perpendicular to them. Other molecules have quite short contacts with Na atoms (starting at ~ 2.2 Å), but this interaction is not reflected in the elongation of the N-N bond, which remains around 1.1 Å. The refined N-N distances in the N_2 units (1.04–1.10 Å) are close to the distances typical for triply bound $\text{N}\equiv\text{N}$ molecule. This suggests that no significant charge transfer occurs between Na and N_2 units, and the formula of the compound may be presented as $\text{NaN}_5\cdot\text{N}_2$. Raman spectrum collected at the position of $\text{NaN}_5 + \text{NaN}_7$ mixture (Fig. S7) has a peak at $\sim 2190\text{ cm}^{-1}$, which is $\sim 200\text{ cm}^{-1}$ lower in frequency than the Raman vibron of $\epsilon\text{-N}_2$ at this pressure. This indicates a very slight elongation of the N_2 molecule embedded into the channels. Apparently no π - π interactions between pentazolate groups are present in $\text{NaN}_5\cdot\text{N}_2$. Therefore, *cyclo-N}_5^- groups in this compound are mainly stabilized by sodium-pentazolate coordination.*

Metal-inorganic frameworks with embedded dinitrogen units $\text{Hf}_4\text{N}_{20}\cdot\text{N}_2$, $\text{WN}_8\cdot\text{N}_2$, $\text{ReN}_8\cdot\text{N}_2$ and $\text{Os}_5\text{N}_{28}\cdot 3\text{N}_2$ were recently synthesized at pressures above 1 Mbar^{22,24} and also predicted in several transition metal compounds³³. These compounds contain polymeric nitrogen chains that serve as linkers in the frameworks. On the example of $\text{NaN}_5\cdot\text{N}_2$ we show that these framework compounds can appear in ionic polynitrides at high pressure too. Therefore, complex inclusion compound is a natural and common form of all kinds of high-pressure polynitrides. The balance between molecular and polymeric nitrogen at high pressure is defined by two factors: the triple $\text{N}\equiv\text{N}$ bond is very stable and has very large internal energy, while single and double bonds are not that strong. At the same time, the dinitrogen molecule with its complete electronic shell usually remains non-bonded, and therefore, has a large volume defined by the van der Waals radius of N. This leads to a significant contribution of the PV term to the enthalpy as the pressure rises. Because of this, the polymerization of bulk nitrogen occurs at $> 100\text{ GPa}$ ³⁴. Below this pressure nitrogen molecule is a stable structural unit and may serve as a template molecule for the self-assembly of the framework structures.

It is likely that due to its complex nature the structure of $\text{NaN}_5\cdot\text{N}_2$ does not emerge in the theoretical predictions of Steele et al.¹¹, who considered structures with up to 16 atoms in the unit cell. Similarly, no such framework compounds were predicted for other alkali-metal polynitrides^{12–14,35}, however, it

is likely that such complex structures may emerge in other ionic metal-nitrogen systems at high pressures.

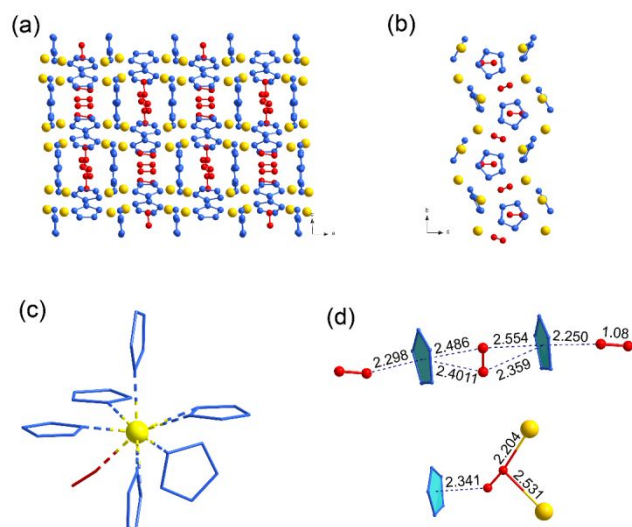


Figure 5. (a,b) Crystal structure of $\text{NaN}_5\cdot\text{N}_2$ in different projections. Na atoms are shown as yellow spheres. Nitrogen atoms forming pentazolate units – blue, dinitrogen molecules – red. (c) Coordination of Na atoms and (d) coordination environments of dinitrogen species. Distances are given in Å. E.s.d. values of bond distances can be found in supplementary cif files.

Stability on decompression

To study the stability region of Na_2N_5 , NaN_5 and NaN_7 the sample was gradually decompressed. NaN_7 could not be well resolved at pressures below 40 GPa. NaN_5 can be detected down to $\sim 18\text{ GPa}$ by Raman spectroscopy, while at the next pressure point ($\sim 13.6\text{ GPa}$) the broad band between 900 and 1200 cm^{-1} disappears (Fig. S8). The crystal quality of NaN_5 becomes worse with decreasing pressure, but the phase can be clearly detected by XRD down to $\sim 25\text{ GPa}$ (Fig. 6a). The strongest Raman peak of NaN_5 (N_5^- breathing mode) remained until $\sim 12\text{ GPa}$ (Fig. 6b).

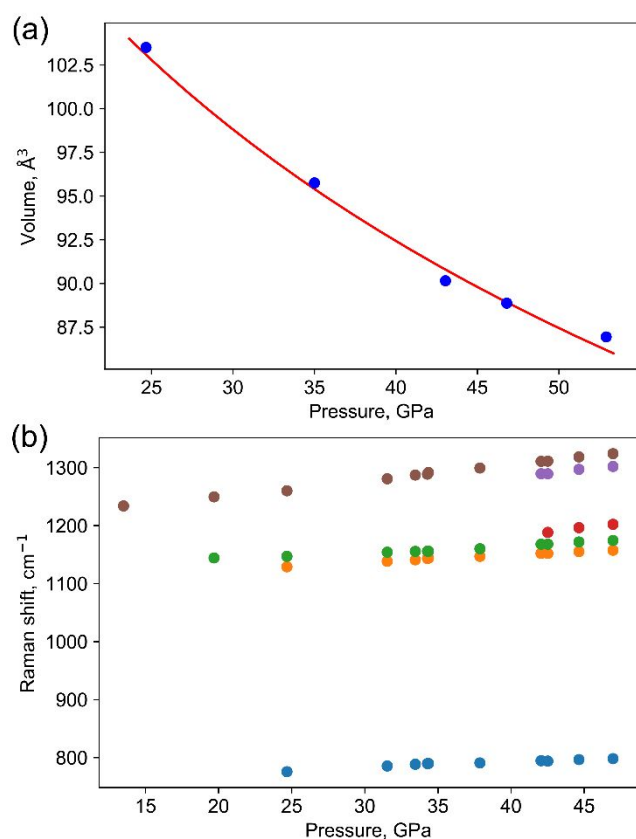


Figure 6. (a) Pressure dependence of the unit cell volume of NaN₃. Red line corresponds to the 2nd order Birch-Murnaghan equation of state with $V_0 = 148.0(4) \text{ \AA}^3$ and $K_0 = 33.0(4) \text{ GPa}$. (b) Pressure dependence of the Raman peaks of NaN₃. With decreasing pressure some peaks could not be resolved anymore.

In our previous studies of NaN₃ at high-pressure high-temperature conditions we performed laser-heating around 27 GPa of a sample without addition of extra nitrogen³⁶. At these conditions, an unusual compound Na₃(N₂)₄ is formed, which has a non-integer formal charge on the dinitrogen unit. In that experiment one could not expect the formation of nitrogen-rich phases with N:Na ratio substantially higher than 3. In the current experiment we explored the possibility of the formation of nitrogen-rich phases in this pressure region by heating NaN₃ with N₂ around 34 GPa. The sample#2 was laser-heated at the very edge of the NaN₃ piece to ensure the excess of nitrogen (Fig. 7a). Single-crystal diffraction analysis of the reaction products at the heated spot evidenced the formation of Na₃(N₂)₄ like in the experiment without extra nitrogen (Table S2). The unit cell volume of Na₃(N₂)₄ is in a good agreement with our previous studies (Fig. 7c). This allows us to conclude that pentazolates cannot be produced from NaN₃ + N₂ even at the excess of nitrogen at pressures below 35 GPa.

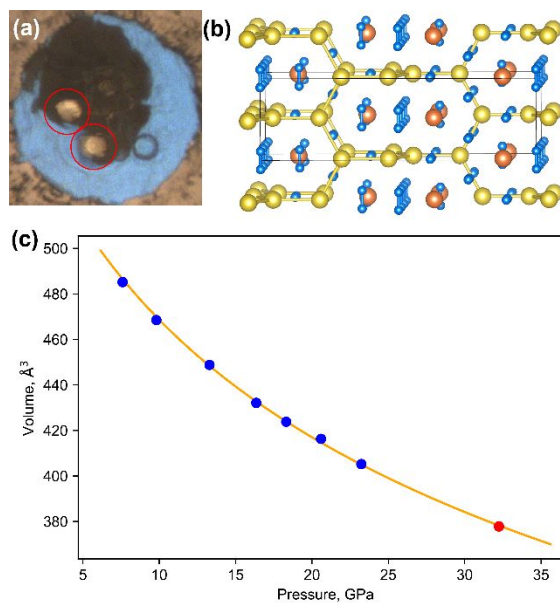


Figure 7. (a) Microscopic image of the sample heated at $\sim 34 \text{ GPa}$. Newly heated areas are shown by red circles. (b) Crystal structure of Na₃(N₂)₄. (c) Pressure dependence of the unit cell volume of Na₃(N₂)₄. Red circle – data from this paper. Blue – from ref.³⁶. Orange line corresponds to the 3rd order Birch-Murnaghan equation of state with $V_0 = 582(6) \text{ \AA}^3$, $K_0 = 28.5(2.8) \text{ GPa}$, $K_0' = 4.4(5)$.

At pressure of 14 GPa laser-heating of NaN₃ with an excess of N₂ leads to a formation of *P4/mmm* NaN₂, previously synthesized at 4 GPa³⁶. As discussed by Holtgrewe *et al.*³⁷ and Bykov *et al.*³⁶ at low-pressure region both X-ray and laser-irradiation induce various photochemical transformations in sodium azide leading to amorphous phases. Therefore, in the previous studies, it was challenging to distinguish between the Raman spectra of the photoinduced products and the Raman spectrum of NaN₂. Here using the combination of X-ray and Raman mapping we could solve this task (Fig. S9). The Raman spectrum of NaN₂ is very simple with two active modes A_{1g} and E_g . The most distinct Raman peak A_{1g} corresponding to the N-N stretching vibration appears at 1960 cm⁻¹ (Fig. S9). The N-N stretching frequency is directly correlated with the N-N bond length following the Badger's rule $d_{NN} \sim Av^{-2/3} + \delta$ ³⁸. The frequency of 1960 cm⁻¹ agrees well with the refined bond distance a [N₂]⁻ unit of 1.16 Å at 4 GPa, demonstrating the charge transfer from Na to N₂ units.

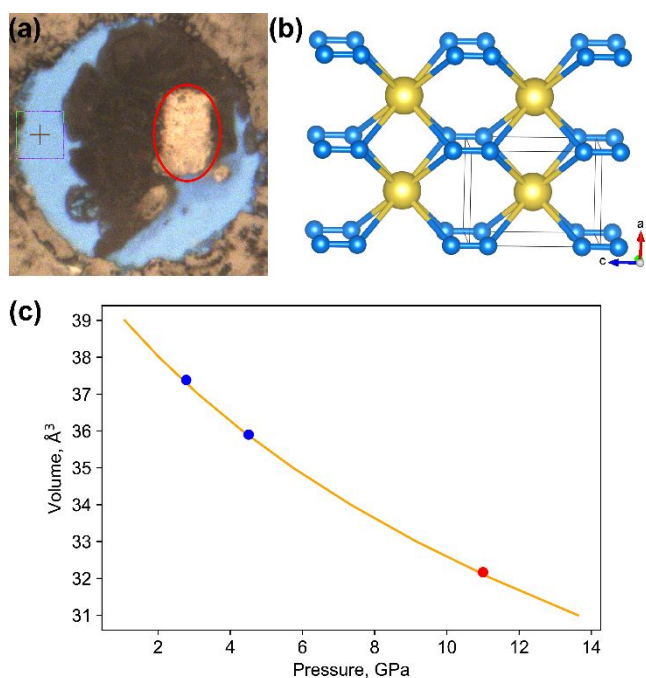


Figure 8. (a) Microscopic image of the $\text{NaN}_3 + \text{N}_2$ sample laser-heated at ~ 14 GPa. Heated area is highlighted. The pressure slightly dropped after heating (b) The crystal structure of NaN_2 . (c) Pressure dependence of the unit cell volume of NaN_2 . Red circle – data from this paper. Blue – from ref. ³⁶. Orange line corresponds to the 2nd order Birch-Murnaghan equation of state with $V_0 = 40.5(1) \text{ \AA}^3$ and $K_0 = 29.1(5) \text{ GPa}$.

Conclusion

In this study we discovered three novel high-pressure compounds in the Na-N system: Na_2N_5 , NaN_5 , and an unprecedented pentazolate framework $\text{NaN}_5 \cdot \text{N}_2$. The transformation diagram in the $\text{NaN}_3 + \text{N}_2$ system can be summarized by the Fig. 9. Formation of metal-pentazolate frameworks through high-pressure self-templating synthesis constitutes a major advance in cyclo-pentazolate chemistry.

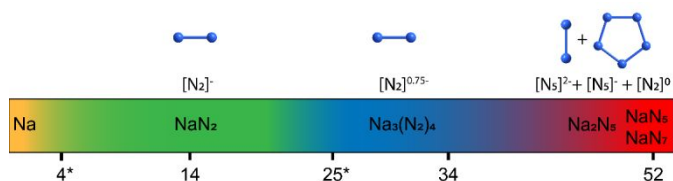


Figure 9. Phases discovered in the $\text{NaN}_3 + \text{N}_2$ system at various pressures. Numbers indicate pressures at which laser-heating was performed (pressure points with asterisks refer to Bykov et al. ³⁶).

Experimental

Synthesis

In all experiments discussed in this article a piece of powder NaN_3 (Sigma Aldrich $\geq 99.5\%$, kept in the dry box) was placed inside a sample chamber of a BX90 diamond anvil cell. Sample #1 was loaded with nitrogen that served as a pressure-transmitting medium and as a reagent, while sample #2 did not contain any pressure-transmitting medium. Both samples were compressed up to ~ 50 GPa and laser

heated ($\lambda = 1064 \text{ nm}$) using the double-sided laser-heating system of GSECARS (13IDD, APS, Argonne, USA). Typical heating time was around 10 s at each heating spot. The summary of experimental conditions is presented in the Table S1.

X-ray diffraction

The reaction products contained multiple good-quality single-crystalline domains of novel phases and they were studied by synchrotron single-crystal X-ray diffraction at the beamline GSECARS 13IDD (APS, Argonne, USA) with the following beamline setup: $\lambda = 0.2952$ or 0.3344 \AA , beam size $\sim 3 \times 3 \mu\text{m}^2$, Pilatus CdTe 1M detector. For the single-crystal XRD measurements samples were rotated around a vertical ω -axis in a range $\pm 33^\circ$. The diffraction images were collected with an angular step $\Delta\omega = 0.5^\circ$ and an exposure time of 2-5 s/frame. For analysis of the single-crystal diffraction data (indexing, data integration, frame scaling and absorption correction) we used the *CrysAlisPro* software package. To calibrate an instrumental model in the *CrysAlisPro* software, *i.e.*, the sample-to-detector distance, detector's origin, offsets of goniometer angles, and rotation of both X-ray beam and the detector around the instrument axis, we used a single crystal of orthoenstatite ($(\text{Mg}_{1.93}\text{Fe}_{0.06})(\text{Si}_{1.93}, \text{Al}_{0.06})\text{O}_6$, *Pbca* space group, $a = 8.8117(2)$, $b = 5.18320(10)$, and $c = 18.2391(3) \text{ \AA}$). Powder diffraction measurements were performed either without sample rotation (still images) or upon continuous rotation in the range $\pm 20^\circ\omega$. The images were integrated to powder patterns with DIOPTAS software³⁹. Le-Bail fits of the diffraction patterns were performed with the Jana2006 software⁴⁰. The structure was solved based on single-crystal XRD data with the ShelXT structure solution program⁴¹ using intrinsic phasing and refined with the Olex2 program⁴². CSD 2051780-2051781 and 2075304 contain the supplementary crystallographic data for this paper. These data can be obtained free of charge from FIZ Karlsruhe via www.ccdc.cam.ac.uk/structures.

Raman spectroscopy

Raman spectra of the samples were collected at GSECARS (Advanced Photon Source, Chicago, USA) Raman system with the excitation wavelength of 532 nm in the spectral range of 10 to 3000 cm^{-1} with a 4 cm^{-1} spectral resolution. Technical details of the system are described elsewhere⁴³.

Calculations details

The structures found in experiment and in previous publications were recalculated with the norm conserving projector augmented waves (PAWs)⁴⁴ and energy cut-off of 750-830 eV using the DFT code CASTEP⁴⁵. CASTEP calculates finite basis set corrections by determining the total energy at three cut-off energies, and then numerically evaluating the derivative required in the correction term. Variational density functional perturbation theory (DFPT)⁴⁶ was used to calculate the Raman spectra. Thirty irreducible k-points were used for electronic Brillouin zone integration and vdW-DF2 dispersion corrections were enabled⁴⁷. Band structure was calculated using PBE functional⁴⁸. The k-point separation was 0.03 \AA^{-1} for conducting and 0.06 \AA^{-1} for insulating systems. The structures were considered converged when the force on each atom was less than 0.002 eV/ Å and total energy tolerance was better than 10^{-6} eV. Deviation of the stress tensor from that defined by the target pressure was less than 0.001 GPa. The phonon dispersion

calculations were performed using a linear response and finite displacements methods implemented in CASTEP⁴⁵ code. Linear response provides an analytical way of computing the second derivative of the total energy with respect to a given perturbation. Spatial derivatives of the macroscopic polarization are calculated numerically along eigenvectors of each Raman active phonon mode by calculating the polarization for each displacement. Raman cross-section were calculated through appropriate space averaging of the spatial derivatives according to the formalism presented in ref. ⁴⁹.

Author Contributions

MB, AG: Conceptualization; MB: Data curation, MB, IB: Formal analysis; AFG, MFM: funding acquisition; MB, EB, SC, VBP, AFG: Investigation; MB, AG: writing

Conflicts of interest

There are no conflicts to declare.

Acknowledgements

Research was sponsored by the Army Research Office and was accomplished under the Cooperative Agreement Number W911NF-19-2-0172. This research used resources of the Advanced Photon Source, a U.S. Department of Energy (DOE) Office of Science User Facility operated for the DOE Office of Science by Argonne National Laboratory under Contract No. DE-AC02-06CH11357. We acknowledge the support of GeoSoilEnviroCARS (Sector 13), which is supported by the National Science Foundation - Earth Sciences (EAR-1634415), and the Department of Energy, Geosciences (DE-FG02-94ER14466).

Notes and references

- 1 Y. Xu, Q. Wang, C. Shen, Q. Lin, P. Wang and M. Lu, *Nature*, 2017, **549**, 78–81.
- 2 C. Zhang, C. Yang, B. Hu, C. Yu, Z. Zheng and C. Sun, *Angew. Chemie - Int. Ed.*, 2017, **56**, 4512–4514.
- 3 C. Zhang, C. Sun, B. Hu, C. Yu and M. Lu, *Science*, 2017, **355**, 374–376.
- 4 Y. Yao, Q. Lin, X. Zhou and M. Lu, *FirePhysChem*, 2021, **1**, 33–45.
- 5 C. Sun, C. Zhang, C. Jiang, C. Yang, Y. Du, Y. Zhao, B. Hu, Z. Zheng and K. O. Christe, *Nat. Commun.*, 2018, **9**, 1269.
- 6 Y. Xu, Q. Lin, P. Wang and M. Lu, *Chem. – An Asian J.*, 2018, **13**, 1669–1673.
- 7 W. Zhang, K. Wang, J. Li, Z. Lin, S. Song, S. Huang, Y. Liu, F. Nie and Q. Zhang, *Angew. Chemie Int. Ed.*, 2018, **57**, 2592–2595.
- 8 D. R. Wozniak and D. G. Piercey, *Engineering*, 2020, **6**, 981–991.
- 9 B. A. Steele, E. Stavrou, J. C. Crowhurst, J. M. Zaug, V. B. Prakapenka and I. I. Oleynik, *Chem. Mater.*, 2017, **29**, 735–741.
- 10 D. Laniel, G. Weck, G. Gaiffe, G. Garbarino and P. Loubeyre, *J. Phys. Chem. Lett.*, 2018, **9**, 1600–1604.
- 11 B. A. Steele and I. I. Oleynik, *Chem. Phys. Lett.*, 2016, **643**, 21–26.
- 12 B. A. Steele and I. I. Oleynik, *J. Phys. Chem. A*, 2017, **121**, 8955–8961.
- 13 A. S. Williams, B. A. Steele and I. I. Oleynik, *J. Chem. Phys.*, 2017, **147**, 234701.
- 14 F. Peng, Y. Han, H. Liu and Y. Yao, *Sci. Rep.*, 2015, **5**, 16902.
- 15 K. Xia, J. Yuan, X. Zheng, C. Liu, H. Gao, Q. Wu and J. Sun, *J. Phys. Chem. Lett.*, 2019, **10**, 6166–6173.
- 16 K. Xia, X. Zheng, J. Yuan, C. Liu, H. Gao, Q. Wu and J. Sun, *J. Phys. Chem. C*, 2019, **123**, 10205–10211.
- 17 Z. Liu, D. Li, F. Tian, D. Duan, H. Li, T. Cui and T. Cui, *Inorg. Chem.*, 2020, **59**, 8002–8012.
- 18 B. Huang and G. Frapper, *Chem. Mater.*, 2018, **30**, 7623–7636.
- 19 H. Zhu, F. Zhang, C. Ji, D. Hou, J. Wu, T. Hannon and Y. Ma, *J. Appl. Phys.*, 2013, **113**, 033511.
- 20 M. Zhang, K. Yin, X. Zhang, H. Wang, Q. Li and Z. Wu, *Solid State Commun.*, 2013, **161**, 13–18.
- 21 M. I. Eremets, M. Y. Popov, I. A. Trojan, V. N. Denisov, R. Boehler and R. J. Hemley, *J. Chem. Phys.*, 2004, **120**, 10618–10623.
- 22 M. Bykov, S. Chariton, E. Bykova, S. Khandarkhaeva, T. Fedotenko, A. V. Ponomareva, J. Tidholm, F. Tasnádi, I. A. Abrikosov, P. Sedmak, V. Prakapenka, M. Hanfland, H.-P. Liermann, M. Mahmood, A. F. Goncharov, N. Dubrovinskaia and L. Dubrovinsky, *Angew. Chemie Int. Ed.*, 2020, **59**, 10321–10326.
- 23 M. Bykov, E. Bykova, G. Aprilis, K. Glazyrin, E. Koemets, I. Chuvashova, I. Kupenko, C. McCammon, M. Mezouar, V. Prakapenka, H.-P. Liermann, F. Tasnádi, A. V. Ponomareva, I. A. Abrikosov, N. Dubrovinskaia and L. Dubrovinsky, *Nat. Commun.*, 2018, **9**, 2756.
- 24 M. Bykov, E. Bykova, E. Koemets, T. Fedotenko, G. Aprilis, K. Glazyrin, H.-P. P. Liermann, A. V. Ponomareva, J. Tidholm, F. Tasnádi, I. A. Abrikosov, N. Dubrovinskaia and L. Dubrovinsky, *Angew. Chemie Int. Ed.*, 2018, **57**, 9048–9053.
- 25 M. Bykov, K. V. Yusenko, E. Bykova, A. Pakhomova, W. Kraus, N. Dubrovinskaia and L. Dubrovinsky, *Eur. J. Inorg. Chem.*, 2019, **2019**, 3667–3671.
- 26 M. Bykov, E. Bykova, A. V. Ponomareva, I. A. Abrikosov, S. Chariton, V. B. Prakapenka, M. F. Mahmood, L. Dubrovinsky and A. F. Goncharov, *Angew. Chemie Int. Ed.*, 2021, **60**, 9003–9008.
- 27 Y. Xu, P. Wang, Q. Lin, X. Mei and M. Lu, *Dalt. Trans.*, 2018, **47**, 1398–1401.
- 28 Y. Xu, P. Wang, Q. Lin and M. Lu, *Dalt. Trans.*, 2017, **46**, 14088–14093.
- 29 H. Xia, X. Qi, W. Zhang, S. Huang, S. Song, Y. Liu, J. Luo and Q. Zhang, *Cryst. Growth Des.*, 2020, acs.cgd.0c01458.
- 30 M. Zhou, S. Liu, M. Du, X. Shi, Z. Zhao, L. Guo, B. Liu, R. Liu, P. Wang and B. Liu, *J. Phys. Chem. C*, 2020, **124**, 19904–19910.

- 31 E. Bykova, M. Bykov, A. Černok, J. Tidholm, S. I. Simak, O. Hellman, M. P. Belov, I. A. Abrikosov, H. P. Liermann, M. Hanfland, V. B. Prakapenka, C. Prescher, N. Dubrovinskaia and L. Dubrovinsky, *Nat. Commun.*, 2018, **9**, 1–8.
- 32 Diamond 4.6.4. Crystal Impact GbR, 1997-2020.
- 33 J. Zhang, A. R. Oganov, X. Li and H. Niu, *Phys. Rev. B*, 2017, **95**, 020103.
- 34 M. I. Eremets, A. G. Gavriluk, I. A. Trojan, D. A. Dzivenko and R. Boehler, *Nat. Mater.*, 2004, **3**, 558–63.
- 35 D. L. V. K. Prasad, N. W. Ashcroft and R. Hoffmann, *J. Phys. Chem. C*, 2013, **117**, 20838–20846.
- 36 M. Bykov, K. R. Tasca, I. G. Batyrev, D. Smith, K. Glazyrin, S. Chariton, M. Mahmood and A. F. Goncharov, *Inorg. Chem.*, 2020, **59**, 14819–14826.
- 37 N. Holtgrewe, S. S. Lobanov, M. F. Mahmood and A. F. Goncharov, *J. Phys. Chem. C*, 2016, **120**, 28176–28185.
- 38 P. L. Holland, *Dalt. Trans.*, 2010, **39**, 5415.
- 39 C. Prescher and V. B. Prakapenka, *High Press. Res.*, 2015, **35**, 223–230.
- 40 V. Petříček, M. Dušek and J. Plášil, *Zeitschrift für Krist. - Cryst. Mater.*, 2016, **231**, 583–599.
- 41 G. M. Sheldrick, *Acta Crystallogr. Sect. A Found. Adv.*, 2015, **71**, 3–8.
- 42 O. V. Dolomanov, L. J. Bourhis, R. J. Gildea, J. A. K. Howard and H. Puschmann, *J. Appl. Crystallogr.*, 2009, **42**, 339–341.
- 43 N. Holtgrewe, E. Greenberg, C. Prescher, V. B. Prakapenka and A. F. Goncharov, *High Press. Res.*, 2019, **39**, 457–470.
- 44 D. R. Hamann, M. Schlüter and C. Chiang, *Phys. Rev. Lett.*, 1979, **43**, 1494–1497.
- 45 S. J. Clark, M. D. Segall, C. J. Pickard, P. J. Hasnip, M. I. J. Probert, K. Refson and M. C. Payne, *Zeitschrift für Krist. - Cryst. Mater.*, 2005, **220**, 567–570.
- 46 K. Refson, P. R. Tulip and S. J. Clark, *Phys. Rev. B*, 2006, **73**, 155114.
- 47 A. Tkatchenko and M. Scheffler, *Phys. Rev. Lett.*, 2009, **102**, 073005.
- 48 J. P. Perdew, K. Burke and M. Ernzerhof, *Phys. Rev. Lett.*, 1996, **77**, 3865–3868.
- 49 D. Porezag and M. R. Pederson, *Phys. Rev. B*, 1996, **54**, 7830–7836.